Int. J. Electrochem. Sci., 17 **(2022)** Article Number: 22049, doi: 10.20964/2022.04.24

International Journal of
ELECTROCHEMICAL
SCIENCE
www.electrochemsci.org

Dye-sensitized solar cells using zinc sulphide-coated titanium dioxide films as photoanode: Effect of immersion temperature on its performance

M.Y.A. Rahman[*], *S.N. Sadikin, A.A. Umar*

Institute of Microengineering and Nanoelectronics (IMEN), Universiti Kebangsaan Malaysia, 43600, Bangi, Selangor, Malaysia
[*]E-mail: mohd.yusri@ukm.edu.my

Received: 29 November 2021 / *Accepted:* 17 January 2022 / *Published:* 4 March 2022

This work is concerned with the utilization of ZnS-coated TiO_2 films as photoanode in a dye-sensitized solar cell (DSSC). The effect of immersion temperature of TiO_2 films in ZnS solution on the optical properties and photovoltaic parameters has been studied. The sample prepared at 50 ^oC of immersion temperature possesess the highest optical reflection which is around 42% in the visible region. The DSSC utilizing the sample prepared at 50 ^oC performed the highest η of 0.28%. This is due to this device owns the the highest optical reflection that means that it has the highest light scaterring.

Keywords: dye-sensitized solar cells, immersion temperature, photoanode, ZnS-coated TiO_2

1. INTRODUCTION

Many ways have been attempted to enhance the properties of TiO_2, namely, doping TiO_2 with metal or non-metal materials assist in improving the performance of dye-sensitized solar cell (DSSC). Metal doping improves the performance of the device by reducing the band gap of TiO_2 and charge transfer resistance at the interface of electrolyte/photoanode, allowing a more efficient electron transport in the photoanode [1-5]. While, non-metal doping in photoanode also assists in improving DSSC efficiency by reducing the recombination of electrons and holes at the interface of photoanode/electrolyte [6,7]. Another effective way of improving the ability of the photoanode to absorb more visible light is by introducing the composite structure of TiO_2 [9].

Chalcogenide material has also been getting interest from researchers as this material can act as compact layer to reduce the recombination reaction at the interface photoanode/electrolyte. In [10,11], the TiO_2-ZnS has been utilized as photoanode of the device and the efficiency has greatly been improved

as compared with the device utilizing pure TiO_2. In this work, TiO_2 has been coated with ZnS. The originality of this work is the preparation of ZnS-coated TiO_2 via simple techniques, namely, liquid phase deposition for preparing TiO_2 and hydrothermal technique for preapring ZnS layer onto TiO_2 films. The goal of this work is to investigate the influence of ZnS immersion temperature of TiO_2 film in ZnS precursor solution on the optical properties and performance of DSSC containing ZnS-coated TiO_2 photoanode. The ZnS precursors are zinc nitrate hexahydrate ($Zn(NO_3)_2$ and thiourea, $(SC(NH_2)_2$.

2. METHODOLOGY

Firstly, the ITO substrates were cleaned by using deionized water, acetone and ethanol for 15 minutes in right sequence in an ultrasonic bath. TiO_2 was deposited on ITO substrates via liquid phase deposition (LPD) method [12]. The cleaned ITO were then immersed in a growth solution containing 0.2 M H_3BO_3 and 0.1 M $(NH_4)_2TiF_6$ at 30 ^oC for 25 hours [12]. Then, ZnS was coated TiO_2 film via hydrothermal technique [14]. TiO_2 samples were immersed in 0.03 M ZnS solution made from dissolving $(Zn(NO_3)_2$ and $(SC(NH_2)_2$ in ethanol at 30 ^oC for 60 minutes [13]. Finally, the prepared samples were then annealed at 400 ^oC for 1 hour in order to make strong adhesion of ZnS on TiO_2 films. These procedures were repeated for preparing ZnS-coated TiO_2 at various immersion temperatures, namely, 50, 60, 70 and 80 ^oC. The ZnS coated TiO_2 films were characterized by UV-Vis spectrometer to study the optical absorption, reflection and energy gap of the samples.

For the fabrication of DSSC, ZnS-coated TiO_2 films were firstly immersed in 0.5 mM of N719 dye solution which acts as a sensitizer for about 15 hours at room temperature. Then, the prepared samples were used as the photoanode in DSSC. The counter electrode of the device was platinum film grown on FTO substrate. The ZnS coated TiO_2 photoanode was then placed on platinum counter electrode. Redox electrolyte containing iodide/triiodide was injected into the 0.23 cm^2 active area of the device. The device was tested in dark and under the illumination of 100 mW cm^{-2} light using Gamry Interface 1000 Potentiostat instrument. The electrochemical properties of the device such as bulk resistance, charge transfer resistance and carrier lifetime were determined by electrochemical impedance spectroscopy (EIS) technique under light illumination.

3. RESULTS AND DISCUSSION

Fig. 1 depicts the optical absorption spectra of ZnS-coated TiO_2 with various immersion temperatures for 60 minutes. According to the figure, all samples absorb light in ultraviolet region which is from 300 to 350 nm. The absorption peak is in the range 325-330 nm which is illustrated in Table 1. The samples with the growth temperatures of 50, 60 dan 70 ^oC possesses the absorption peak at the wavelength of 325 nm, while the samples with the immersion temperature of 30 dan 80 ^oC own the absorption peak at the wavelength of 330 nm. The samples do not exhibit the absorption peak in the visible region since TiO_2 and ZnS are only able to absorb light in ultraviolet region [14,15]. Nevertheless, TiO_2 still can absorb light in visible region but with low fraction [16]. ZnS is able to absorb light in

visible region by varying its annealing temperature that causes its defects in its structure such as Zn atau S vacancies as reported in [17]. It is observed that *blue shift* phenomena occurs when the growth temperature was increased from 30 to 50 ^{o}C corresponding with the absorption peak change from 330 to 325 nm. This is due to the increment in energy gap with the increase in growth temperature.

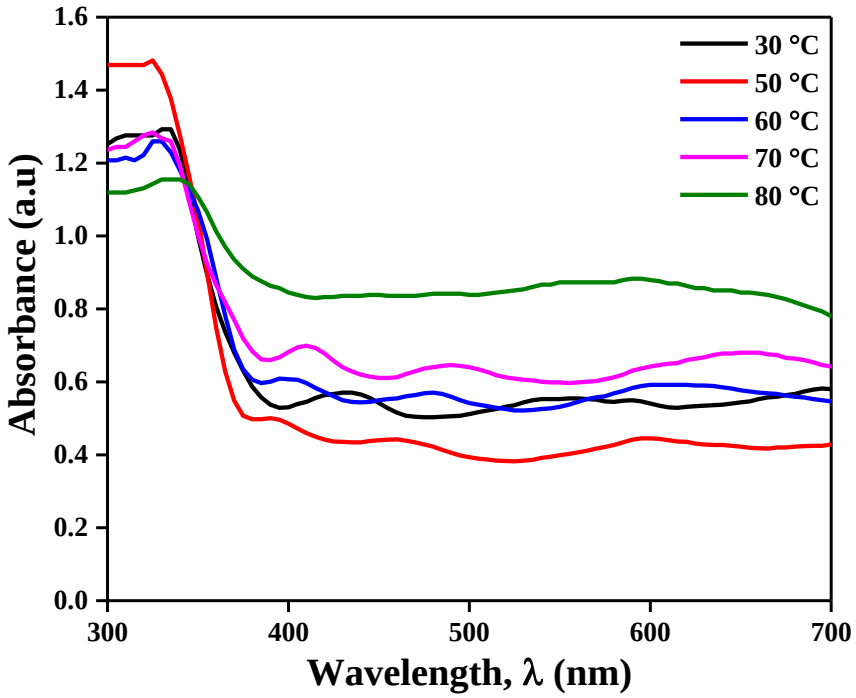

Figure 1. Optical absorption spectra of ZnS-coated TiO_2 with various growth temperatures of ZnS

Fig. 2 illustrates the reflection spectra of the samples with various growth temperatures of ZnS. According to the figure, the reflection of the samples is found to increase with the growth temperature until 50 ^{o}C and then decreases when the temperature was further increased to 60, 70 and 80 ^{o}C. The highest reflection belongs to the sample with the growth temperature of 50 ^{o}C, that is 42%, while the lowest reflection belongs to the sample grown at 80 ^{o}C that is 14.8%. All samples exhibit high reflection in visible region. By comparison of Fig. 1 with Fig. 2, it is found that the sample with the lowest absorption in visible region posseses the highest reflection in the same region. The sample with highest absorption in visible region has the lowest reflection in the same region. In other words, high absorption results in low reflection. The sample that has high diffuse reflection possesess high light scaterring ability which will consequently improve the DSSC performance [18]. This is because high light scaterring will increase the optical pathway in the sample [19]. Nevertheless, at the growth temperature of 60, 70 dan 80 ^{o}C, the diffuse reflection has been found to decrease until 14.8%.

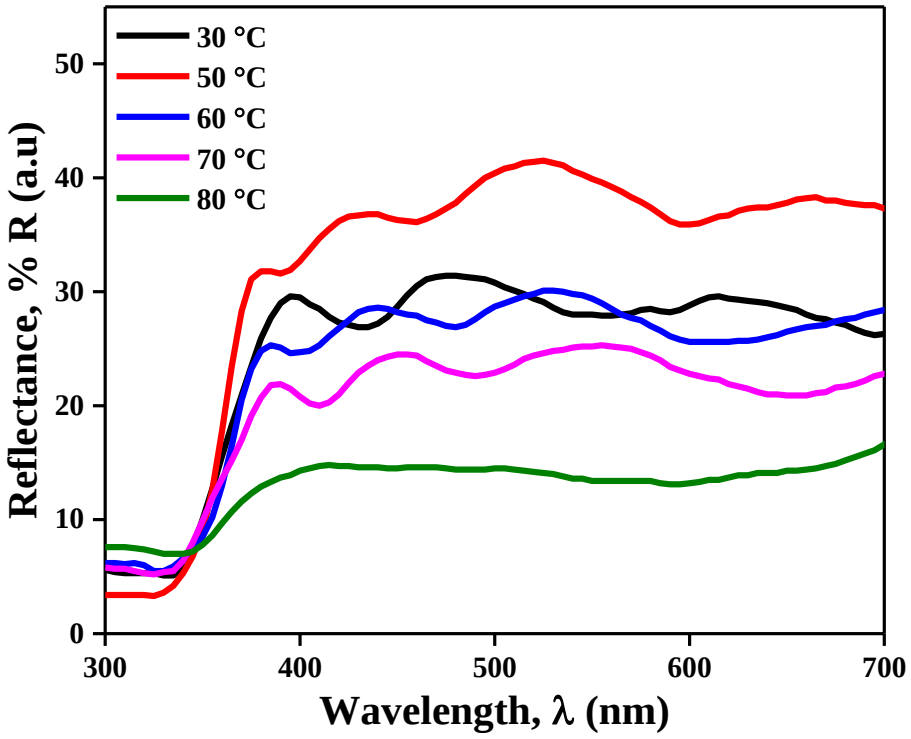

Figure 2. Diffuse reflection spectra of ZnS-coated TiO_2 with various growth temperatures of ZnS

Fig. 3 shows the Tauc plots of the samples with various immersion temperatures of ZnS. The plots are used to compute the energy gap for each sample. Firstly, a tanget line is drawn at higher and lower part of each plot. Then, a vertical line is drawn from the intersection point of the two tangent lines, extending to hv axis. The energy gap is then estimated and presented in Table 1. According to Table 1, the energy gap increases with temperature until 50 ^{o}C. The energy gap remains unchanged when the temperature was increased to 60 and 70 ^{o}C. The energy gap drops when the temperature was further increased to 80 ^{o}C.

Fig. 4 displays the *I-V* curves in dark for the device utilizing the samples with various growth temperatures of ZnS. According to the figure, the device with the immersion temperature of 30 and 50 ^{o}C possesses the highest leak current. While, the device utilizing uncoated ZnS sample owns the lowest leak current followed by the device with the growth temperature of 80 ^{o}C. The device utilizing the sample grown at 60 and 70 ^{o}C shares the second lowest leak current as depicted in Figure 3. High leak current indicates high recombination rate between electron and hole in the device. The growth rate of ZnS on TiO_2 deposited on ITO substrate affects the magnitude of leak current in DSSC as reported in [20]. The unexposed ITO which is not covered by ZnS-coated TiO_2 coated N719 dye is in contact with the redox electrolyte cause the recombination between electron and hole at the interface of ITO/electrolyte instead of the recombination between the electrons injected into the conduction band of TiO_2 and holes in the electrolyte. Such recombination affects the charge transfer resistance at the interface of electrolyte/N719/ZnS/TiO_2 (R_{ct2}).

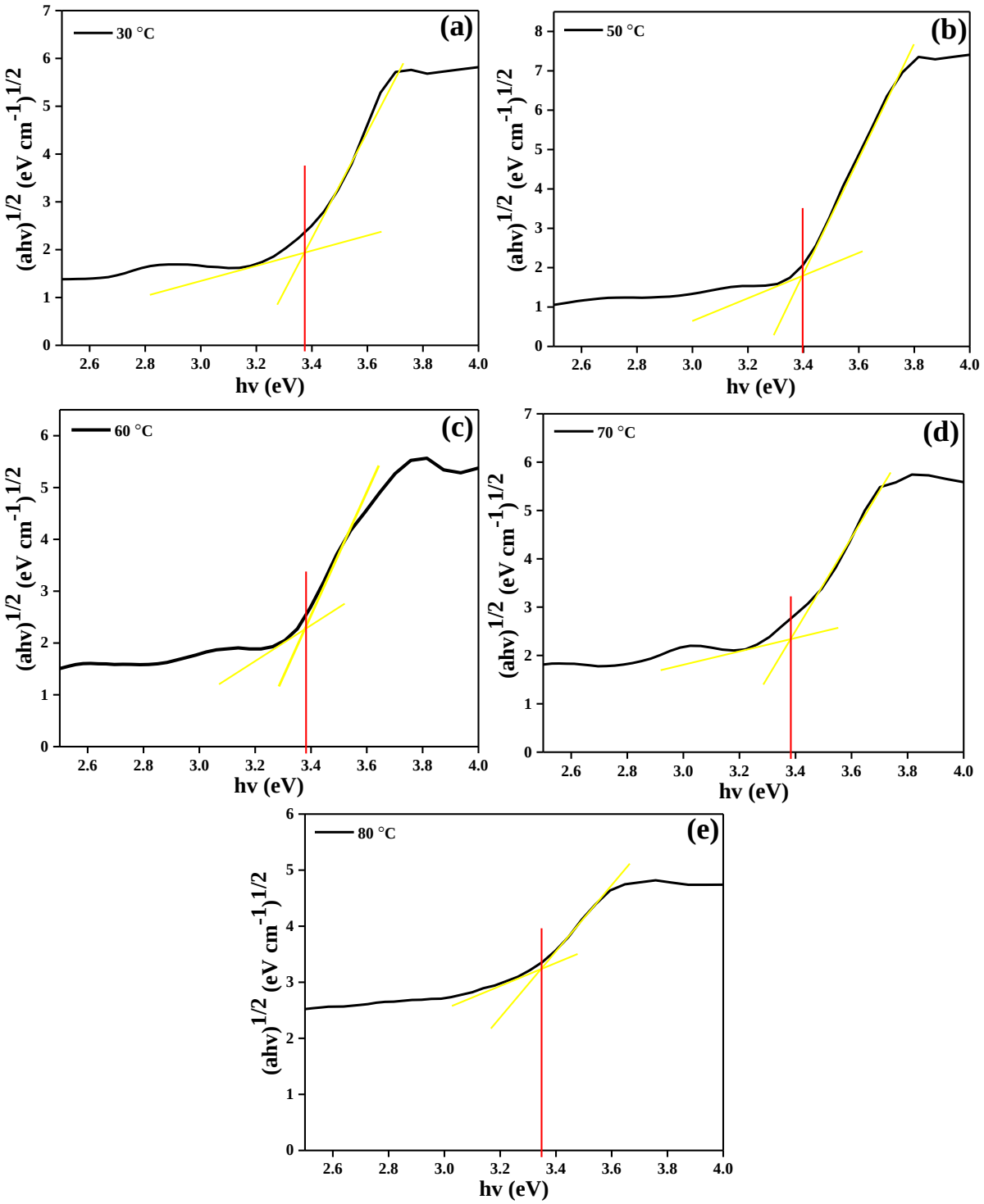

Figure 3. Tauc plots of ZnS-coated TiO_2 with various growth temperatures of ZnS

Table 1. Peak absorption and energy gap of ZnS-coated TiO_2 with various growth temperatures of ZnS

Growth temperature (◦C)	Absorption peak (nm)	Energy gap (eV)
30	330	3.37
50	325	3.39
60	325	3.39
70	325	3.39
80	330	3.35

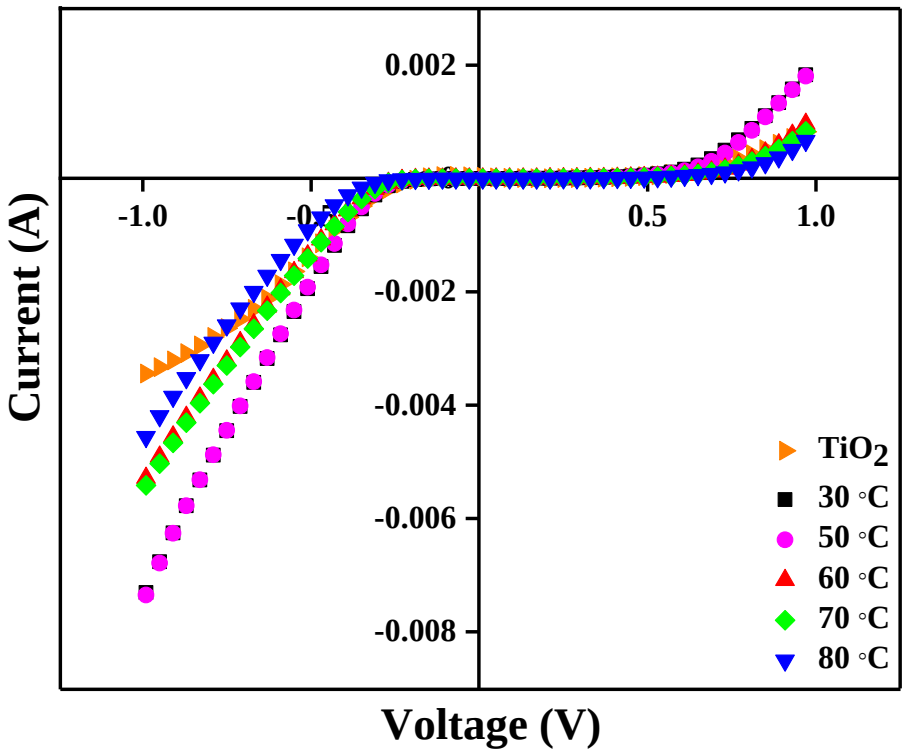

Figure 4. *I-V* curves in dark of the DSSC utilizing pure TiO_2 and ZnS-coated TiO_2 with various growth temperatures of ZnS

Fig. 5 shows the *J-V* curves of the device utilizing the uncoated and ZnS-coated TiO_2 samples with various immersion temperature of ZnS. According to the curves, the shape of the curves are similiar to that reported in our previous work [21,22]. The photovoktaic parameters such as J_{sc}, V_{oc}, *FF* and η are extracted from Fig. 5 and summarized in Table 2. According to the table, the device with 50 ◦C has the highest J_{SC} that is 1.07 mA cm^{-2}, followed by the device with the sample grown at the temperature of 60, 70, 30 and 80 ºC. The device with the immersion temperature of 50 ◦C demonstrates the highest η that is 0.28%, followed by the device utilizing the sample with the immersion temperature of 60, 70, 30 and 80 ºC. The highest V_{oc} of 0.64 V belongs to the device with the sample with the immersion

temperature of 60 and 70 °C. Meanwhile, the highest *FF* that is 0.48 is owned by the device with the immersion temperature of 30, 60 and 70 °C. The lowest $V_{oc,}$ *FF* and η belongs to the device utilizing uncoated sample. Increasing the immersion temperature is found to improve the J_{sc}, $V_{oc,}$ and η. However, according to the photovoltaic parameters presented in Table 2, the J_{sc} and η decrease once the immersion temperature was further increased to 60 °C. For $V_{oc,}$ its value drops once the annealing temperature was further increased to 80 °C. Also, at 80 °C, the η drops to 0.21 % which is the lowest among the devices utilizing ZnS-coated TiO_2 with various immersion temperatures. However, this η is still higher than that of the device utilizing pure TiO_2 photoanode that is 0.13%. The device with the immersion temperature of 50 °C demonstrates the highest η due to this sample has the highest diffuse reflection as depicted in Fig. 2. On the other hand, the device utilizing pure TiO_2 owns the lowest η which is caused by the highest R_{ct1} and R_{ct2} as illustrated in Table 2. It is also due to this device has the shortest τ as summarized in Table 2.

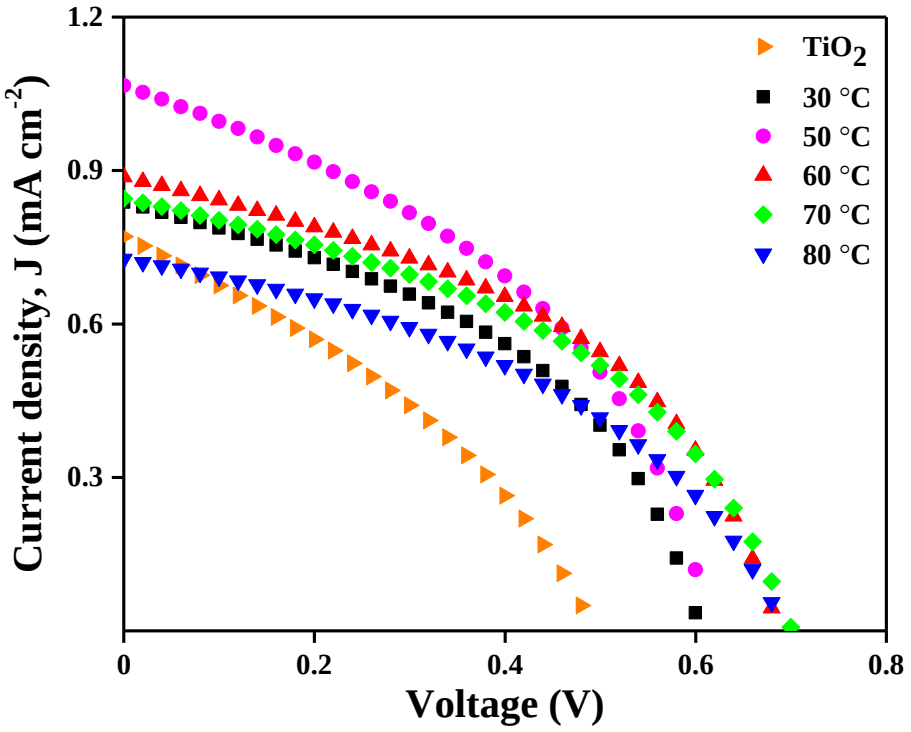

Figure 5. *J-V* curves under illumination of 100 mW cm^{-2} light of the device utilizing pure TiO_2 and ZnS-coated TiO_2 with various growth temperatures of ZnS

Fig. 6 illustrates the Nyquist plots of the devices utilizing the samples with various growth temperatures. According to Figure 6, the plot of all devices display two semicircles for which the first semicircle in high frequency region denotes the charge transfer resistance at the interface of Pt/electrolyte (R_{ct1}). The second semicircle which is in low frequency region represents the charge transfer resistance at the interface of electrolyte/N719/ZnS/TiO_2 (R_{ct2}). Both resistances are presented in Table 2. According to Table 2, there is neither increasing nor decreasing trend of R_{ct1} and R_{ct2} with

immersion temperature. It is found that the value of R_{ct2} is higher than that of R_{ct1} for all devices. This indicates that the oxidation rate occuring at the interface of electrolyte/N719/ZnS/TiO_2 is faster than that of reduction rate taking place at the interface of Pt/electrolyte. In other words, the reduction of triodide to iodide is faster than the oxidation of iodide to triiodide and the regeneration of the oxidized dye molecule to the dye molecule at ground state. Also according to Table 2, the device with 30 ^oC sample owns the lowest R_{ct1}, followed by the device utilizing 80, 60, 50, 70 ^oC and pure TiO_2 samples. For R_{ct2}, the device with 60 ^oC sample has the lowest value, followed by the device utilizing 30, 50, 80, 70 ^oC and pure TiO_2 samples.

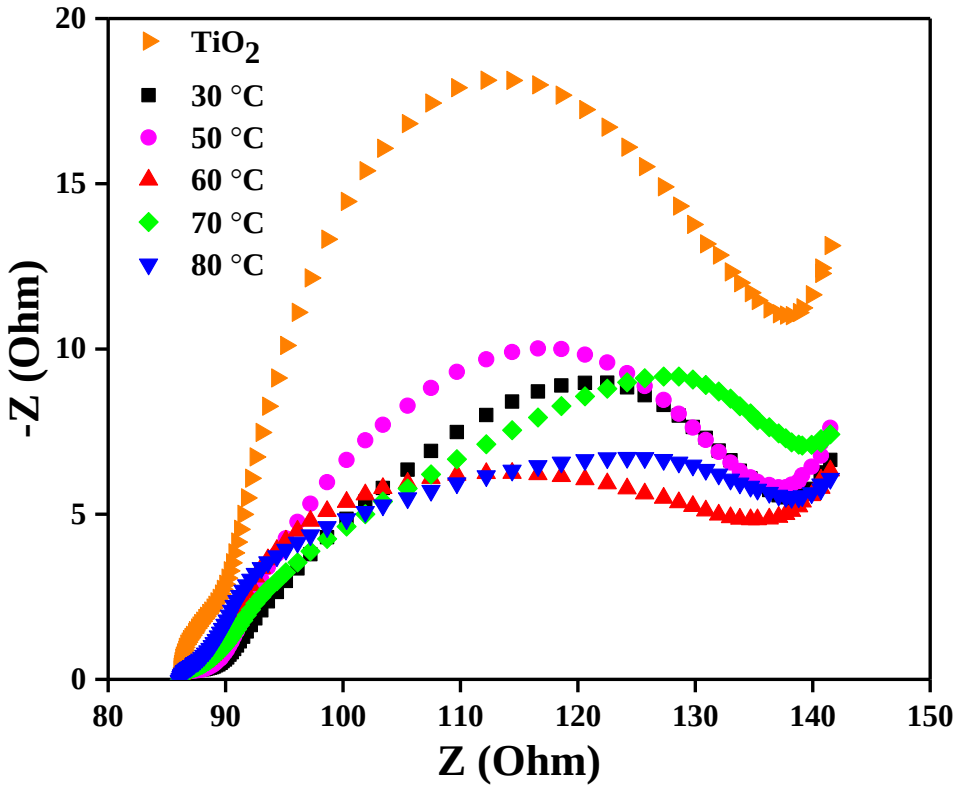

Figure 6. Nyquist plots under illumination of 100 mW cm^{-2} light of the devices utilizing pure TiO_2 and ZnS-coated TiO_2 with various growth temperatures of ZnS

Finally, Fig. 7 shows the Bode plots for all devices which are used to compute the carrier lifetime (τ**)**. Each plot shows a peak frequency which is then used to calculate the carrier lifetime and presented in Table 2. According to the table, the device using the sample with the immersion temperature of 60 ^oC has the longest τ, followed by the device with the immersion temperature followed by the samples with the immersion temperature of 80, 70, 30 and 50 ^oC. These devices own higher $\boldsymbol{\tau}$ than the device utilizing pure TiO_2.

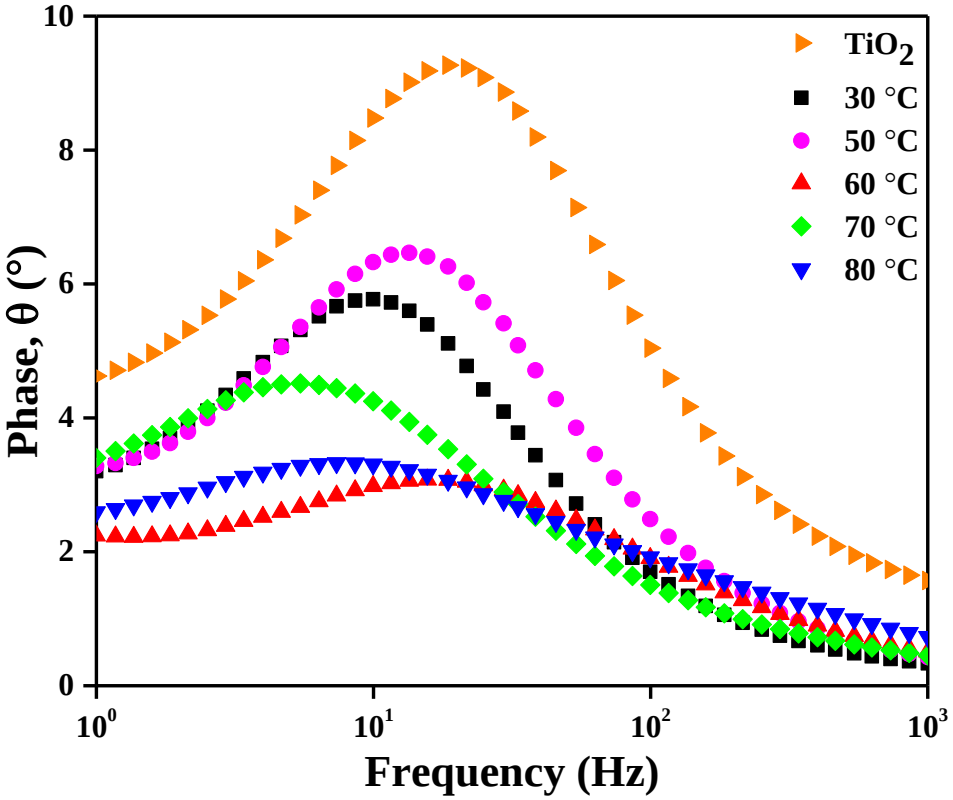

Figure 7. Bode plots under illumination of 100 mW cm^{-2} light of the devices utilizing pure TiO_2 and ZnS-coated TiO_2 with various growth temperatures of ZnS

Table 2. Photovoltaic and EIS parameters of the device with various ZnS growth temperatures

Growth temperature (°C)	J_{sc} (mA cm^{-2})	V_{oc} (V)	*FF*	η (%)	R_{ct1} (Ω)	R_{ct2} (Ω)	τ (ms)
TiO_2	0.78	0.42	0.40	0.13	1.80	55.2	0.11
30	0.84	0.56	0.48	0.23	0.30	23.7	0.17
50	1.07	0.61	0.42	0.28	0.80	26.1	0.16
60	0.89	0.64	0.48	0.27	0.70	21.5	0.32
70	0.85	0.64	0.48	0.26	1.00	30.2	0.22
80	0.73	0.62	0.47	0.21	0.60	27.7	0.30

The highest η obtained from this work that is 0.28% is lower than that reported in our previous work which reported the η of 0.80 and 1.32%, respectively [13,23]. It is lower than that of the device utilizing graphene-coated TiO_2, demonstrating the η of 1.47% [24]. This is because the R_{ct2} is higher than that reported in [13,23]. This is also due to the carrier lifetime in this work is shorter than those reported in [13,23]. It is lower than that of the device utilizing TiO_2-CdS for which its efficiency was 1.44% [11]. However, it is also lower than that of the device employing TiO_2/ZnO which demonstrated the η of 0.62% [25].

4. CONCLUSIONS

ZnS-coated TiO_2 films with various immersion temperatures were prepared via liquid phase deposition and immersion techniques. The samples were then utilized as photoanode in DSSC. The optical absorption, refelction and energy gap are influenced by the immersion temperature of ZnS. The efficiency increases as the immersion temperature is increased and achieved the optimum efficiency at the immersion temperature of 50 ^{o}C min with the η of 0.28% corresponding with the J_{sc} of 1.07 mA cm^{-2} and V_{oc} of 0.61 V, respectively. This is due to this device has the highest diffuse reflection in visible region.

ACKNOWLEDGEMENT
The authors would like to thank Universiti Kebangsaan Malaysia for providing financial support to carry out this work through research grant, FRGS/1/2019/STG02/UKM/02/1.

References

1. J. Zhang, W. Peng, Z. Chen, H. Chen, L. Han, and J. Phys. Chem., 116 (2012) 19182.
2. V. Kumar, N. Singh, L.P. Purohit, A. Kapoor, O.M. Ntwaeaborwa and H.C. Swart, *J. Appl. Phys*., 114 (2013) 134506.
3. J.J. Teh, S.L. Ting K.C. Leong, J. Li and P. Chen, *ACS Appl. Mater. Interf*., 5 (2013) 11377.
4. S. Ameen, M.S. Akhtar, H.K. Seo, Y.S. Kim and H.S. Shin, *Chem. Eng. J*., 187 (2012) 351.
5. F. Giordano, A. Abate, J.P.C. Baena, M. Saliba, T. Matsui, S.H. Im, S. M. Zakeeruddin, M.K. Nazeeruddin, A. Hagfeldt and M. Graetzel, *Nature Comm*., 7 (2016) 10379.
6. Q. Sun, J. Zhang, P. Wang, J. Zheng, X. Zhang, Y. Cui, J. Feng and Y. Zhu, *J. Renew. Sustain. Energy*, 4 (2012) 023104.
7. T. Ma, M. Akiyama, E. Abe and I. Imai, *Nano Lett*., 5 (2005) 2543.
8. Y.I. Feng, J. Chen, X. Huang, W. Liu, Y. Zhu, W. Qin and X. Mo, *Crystal Res. Tech*., 51 (2016) 548.
9. R. Raja, M. Govindaraj, M.D. Antony, K. Krishnan, E. Velusamy, A. Sambandam, M. Subbaiah and V.W. Rayar, *J. Solid State Electrochem*., 21 (2016) 891.
10. S.S. Rao, D. Punnoose, C.V. Tulasivarma, C.H.S.P. Kumar, C.V.M. Gopi, S.K. Kim and H.J. Kim, *Dalton Trans*. 44 (2015) 2447-2455.
11. H.J. Kim, J.H. Kim, I.K. Durga, D. Punnoose, N. Kundakarla, A.E. Reddy and S.S. Rao, *New. J. Chem*., 40 (2016) 9176.
12. A. A. Umar, M. Y. A. Rahman, S.K.M. Saad, M.M. Salleh and M. Oyama, *Appl. Surf. Sci*., 270 (2013) 109.
13. S.N. Sadikin, M.Y.A. Rahman and A.A. Umar, *Superlatt. Microstruct*., 130 (2019) 153.
14. M.B. Karoui, Z. Kaddachi and R. Gharbi, *J. Phys.: Conf. Ser*., 596 (2015) 012012.
15. V. Štengl, S. Bakardjieva, N. Murafa, V. Houšková and K. Lang, *Micropor. Mesopor. Mater*., 110 (2008) 370.
16. M. Szindler, P. Boryło and T. Jung, *Open Phys*., 15 (2017) 1067.
17. N. Shanmugam, S. Cholan, N. Kannadasan, K. Sathishkumar and G. Viruthagiri, *J. Nanomater*., 2013 (2013) 351798.
18. V. Karthikeyan, S. Maniarasu, V. Manjunath, E. Ramasamy and G. Veerappan, *Sol. Energy*, 147 (2017) 202.
19. M. Jeng, Y.L. Wung, L.B. Chang and L. Chow, *Int. J. Photoenergy*, 2013 (2013) 563897.

20. K. Zhu, N. Kopidakis, N.R. Neale, J. Van De Lagemaat and A.J. Frank, *J. Phys. Chem*. B., 110 (2006) 25174.
21. S.N. Sadikin, M.Y.A. Rahman and A.A. Umar, *Optik*, 211 (2020) 164644.
22. U.A. Kamarulzaman, M.Y.A. Rahman, M.S. Su'ait and A.A. Umar, *Optik*, 218 (2020) 164976.
23. M.Y.A. Rahman, S.N. Sadikin and A.A. Umar, *Appl. Phys. A*, 124 (2018) 460.
24. S.N. Sadikin, M.Y.A. Rahman, A.A. Umar and T.H.T. Aziz, *Superlatt. Microstruc*., 128 (2019) 92.
25. S.A.M. Samsuri, M.Y.A. Rahman, A.A. Umar and M.M. Salleh, *Mater. Lett.*, 160 (2015) 388.